ACS Photonics, Volume 9, Issue 12, December 2022, pp. 3917-3925
DOI:10.1021/acsphotonics.2c01235

Enhancing large-area scintillator detection with photonic crystal cavities

Wenzheng Ye[1,2], Gregory Bizarri[3], and Muhammad D. Birowosuto[4]*, Liang Jie Wong[1,2]*

[1]School of Electrical and Electronic Engineering, Nanyang Technological University, 50 Nanyang Avenue, Singapore 639798, Singapore

[2]CNRS-International-NTU-THALES Research Alliance (CINTRA), Nanyang Technological University, 50 Nanyang Drive, 637553, Singapore

[3]Cranfield University, Bedfordshire, MK43 0AL, England

[4]Łukasiewicz Research Network-PORT Polish Center for Technology Development, Stabłowicka 147, 54-066 Wrocław, Poland

*Email: muhammad.birowosuto@prasetiyamulya.ac.id

*Email: liangjie.wong@ntu.edu.sg

KEYWORDS: scintillators, nanophotonics, Purcell effect, spontaneous emission, high energy particles

ABSTRACT: Scintillators are materials that emit visible photons when bombarded by high energy particles (X-ray, gamma ray, electrons, neutrinos, etc.), and are crucial for applications including X-ray imaging and high energy particle detection. Here, we show that one-dimensional (1D) photonic crystal (PhC) cavities – added externally to scintillator materials – can be used to tailor the intrinsic emission spectrum of scintillators via the Purcell effect. The emission spectral peaks can be shifted, narrowed or split, improving the overlap between the scintillator emission spectrum and the quantum efficiency (QE) spectrum of the photodetector. As a result, the overall photodetector signal can be enhanced by over 200%. The use of external PhC cavities especially benefit thick and large-area scintillators, which are needed to stop particles with ultrahigh energy, as in large-area neutrino detectors. Our findings should pave the way to greater versatility and efficiency in the design of scintillators for applications including X-ray imaging and positron emission tomography.

Introduction

High energy particles undergo a variety of interactions when incident upon scintillators, including Compton scattering, electron-positron pair formation, electron ionization and recombination of electron-hole pairs at luminescence centers. The last process is directly useful in the detection of high energy particles as it produces light that can then be captured by photodetectors such as photomultiplier tubes (PMT)[1] or avalanche photodiodes (APD)[2]. Scintillation, which refers to the generation of light in a material (known as a scintillator) from incident high energy particles, plays a vital role in many technologies including positron emission tomography (PET)[3, 4], medical and industrial computed tomography (CT)[5], security scanning[6], neutrino detection[7-11] and radioluminescence microscopy[12].

Crucial to the performance of scintillators are their response times (as small as possible) and efficiencies (as large as possible). Approaches to improve these properties include engineering the scintillator's atomic composition[13, 14] and developing new materials[14-19] to optimize the decay rate and scintillator efficiency. Other approaches include implementing the scintillator as a thin film[20] and adding photonic crystals (PhCs) as coatings[21-23] to enhance the photon extraction efficiency. In the latter case, PhCs are only used to manipulate the already-created scintillation emission, as opposed to the intrinsic emission properties. In a series of recent, exciting research breakthroughs, it was shown that structuring the scintillator material itself into a PhC can enhance the intrinsic emission process through the Purcell effect[24], resulting in improved scintillation efficiency.[25-27] However, the impact of externally added PhC structures on the intrinsic emission process has not been explored.

In this work, we show via numerical simulation that external large-area PhC cavities can enable over 200% enhancement of the overall photodetector signal (The photodetector signal enhancement is defined as the ratio of the photoelectron number detected at the photodetector with the PhC cavity to that without PhC cavity). This enhancement occurs because the external PhC cavity shapes the scintillator's emission spectrum via the Purcell effect, resulting in an improved overlap between the emission spectrum and the quantum efficiency (QE) spectrum of the photodetector. This enhances the rate of photoelectron generation and hence the overall photodetector signal. To study this enhancement, we present a theory that takes into consideration the fact that dipoles in different positions have different decay rates, as well as the decay of the dipole density with depth from the scintillator surface. Our theory is suitable for studying large-area detectors, whose

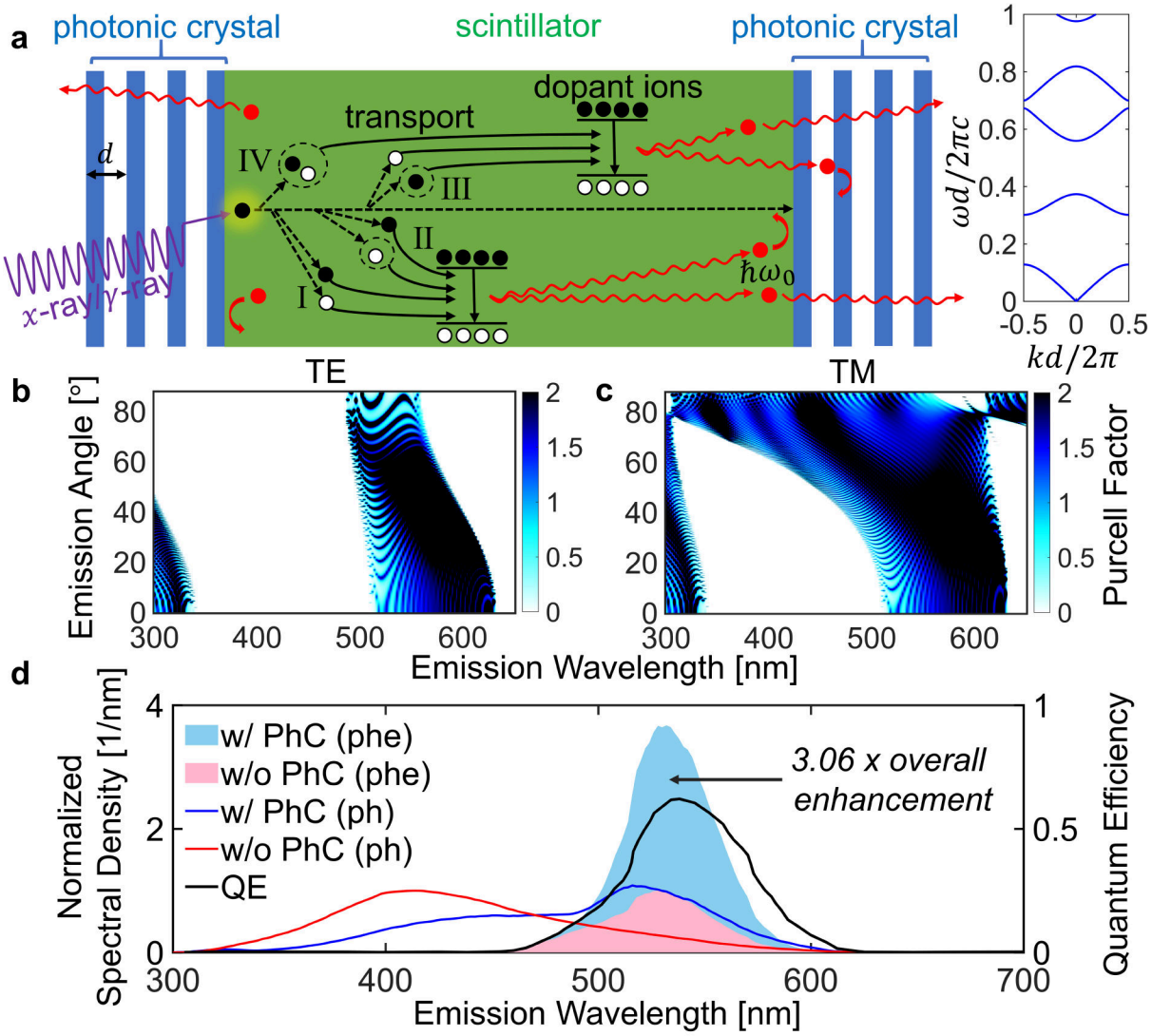

Figure 1. Enhancing high-energy particle detection with external photonic crystal (PhC) cavities. (a) Illustration of the scintillation process in activated scintillator: an incident high energy particle creates a primary electron (glowing black circle), which in turn creates secondary electrons (black circles) and holes (white circles). The dotted circles in processes II, III and IV indicate trapped holes, trapped electrons, and self-trapped excitons, respectively. Visible light is emitted by the recombination of electron-hole pairs in the dopant ions through spontaneous emission. The spontaneous emission properties can be tailored by the PhC band structure (inset), where k, ω, d denote the wavevector magnitude in air, angular frequency, and PhC period, respectively. (b) & (c) Purcell factor as a function of emission wavelength and emission angle (in air) for a dipole located at the middle of the scintillator (CsI:Na). The Purcell factor is suppressed within the bandgap (white area) of the PhC but enhanced by some fringe-like TE and TM modes within the energy bands of the PhC. (d) Enhancing photoelectron number at the photodetector by tailoring the emission spectrum of scintillator (thick film CsI:Na) with an external PhC cavity. The solid lines and shaded areas denote the spectral density of photons (ph) and photoelectrons (phe), respectively, normalized to the respective spectra peaks for the case without PhC cavity. The PhC is composed of alternating layers of dielectric material (refractive index 5) and air. The emission spectrum is tailored via Purcell effect, resulting in an improved overlap between the emission spectrum and the quantum efficiency (QE) spectrum of the photodetector, achieving 3.06 times enhancement in the overall detected photoelectron number.

transverse dimensions are typically at least 10-100 times larger compared to the structure's thickness, making a 1D model[28] a good approximation. Such large-area detectors are used in many applications including X-ray imaging, security scanning and dark matter detection.[6, 29, 30] In particular, our numerical results show that the 1D PhC cavities can be designed to shift, narrow and split peaks of the scintillator emission spectrum. Compared to structuring the scintillator material directly into PhCs, externally added PhC cavities benefit from a wider range of materials available for realizing the PhCs, allowing for a smaller number of layers and therefore less vulnerability to fabrication error. Furthermore, using external PhC cavities avoids modifying the scintillator material itself in the event that such modifications are challenging or impractical: for instance, when thick scintillators are needed to stop photons with ultrahigh energy, as in large-area neutrino detectors[7-11].

Results

Figure 1 shows a thick single-crystal scintillator sandwiched between two PhCs of the same design – we refer to this PhC sandwich as a PhC cavity. Ionizing radiation (e.g., X-ray, gamma rays) are converted into charged particles (e.g., hot electrons and holes) by processes like the photoelectric effect, Compton scattering, and pair production as they pass through the scintillator and dielectric materials.[15, 31-34] These charged particles lose their energy through the creation of multiple less energetic electrons and holes. The electrons and holes can form excitons that later relax radiatively to emit photons, or non-radiatively to heat, or transfer primarily to the dopant ions. Independent electrons and holes can also transfer energy to the dopant ions. The resulting excited dopant ions can then relax to its ground state either radiatively or not. The branching ratio between the processes associated with charged particle energy loss is dependent on the properties of the host excitons, dopant ions (i.e., type, concentration) and host defects.

Scintillators are self-activated if they rely mainly on the host exciton for emission, and activated if they rely on the dopant ions for emission. Self-activated scintillators have exciton emission lifetimes varying from few picoseconds to microseconds.[35, 36] The 5d-4f transitions of Lanthanide doped scintillators, an example of activated scintillators, have a primary decay component of several tens or hundreds of nanoseconds.[37-39] Scintillation in activated scintillators involves three main mechanisms in Figure 1a: 1) direct electron-hole capture by dopant ions (energy transfer mechanism I), which takes place on a timescale of < 1 ns; 2) delayed electron and hole capture due to metastable electron and/or hole trapping at defect sites (energy transfer mechanisms II and III), with transfer rates and efficiencies determined by defect characteristics. Electron and/or hole trapping can lead to delayed excitation of the dopant ions, which could result in lifetimes longer than the intrinsic lifetime of the dopant ions; 3) dipole transfer from self-trapped excitons (STEs) to dopant ions (energy transfer mechanism IV) with transfer rates and efficiencies determined by STE/dopant ion affinity, which once again could result in lifetimes longer than the intrinsic lifetime of the dopant ions.[40] Regardless of the energy transfer mechanism, an electron-hole pair captured in a dopant ion will recombine and emit a photon or decay non-radiatively.

The impact of adding an external PhC cavity is twofold: Firstly, the PhC cavity affects the intrinsic dipole decay rate in the scintillators via the Purcell effect and thus tailors the intrinsic emission spectrum of dipole emitters. The Purcell effect is dependent on the local density of states (ρ_p) constructed by the photonic crystal cavity, i.e., $\gamma \propto \rho_p(\boldsymbol{r}, \omega)$, where $\gamma, \boldsymbol{r}, \omega$ are the Purcell factor, dipole position, and emission angular frequency, respectively. Secondly, the PhC cavity further shapes the emitted photons through the transmission coefficient of the internal photons into the external environment where they are captured by the photodetector.

Our theory follows the derivations in Ref[25], with the following key differences that are crucial for accuracy in the scenario that we consider:

(a) Our model takes into consideration the fact that dipoles in different positions have different decay rates.

(b) We consider the spectral dependence of the scintillator's emission and photodetectors' quantum efficiency.

(c) We consider the absorption of high energy particles by both dielectric and scintillator materials.

(d) We do not assume a uniform dipole distribution, but instead consider an exponential decay with the depth from the scintillator surface.

Full details of our theory are provided in the Methods and Supporting Information (SI) Section I. In particular, Figure S5 in SI Section I. C illustrates the importance of considering the ability of the PhC cavity to modify the intrinsic emission spectrum via the Purcell effect, in addition to affecting the transmission of photons after they have been emitted.

The external photonic crystal cavity affects the scintillator dipole decay rate via the Purcell effect and reshapes the emission spectrum. The Purcell factor $\gamma(\omega, \theta, \sigma)$ for a dipole located at the center of the scintillator is presented in Figure 1b and 1c, which shows the suppression in the bandgap region and the enhancement in some modes within the energy bands. Here ω denotes the emission angular frequency, θ denotes the emission angle in vacuum, σ denotes the emission polarization. Based on spontaneous emission process described by Einstein's coefficient and the transmission of photons shaped by PhC cavity, the photon number is suppressed and enhanced in the bandgap and some modes within the energy bands, respectively. It leads to the better match between emission spectrum of the scintillator and QE spectrum of the specific photodetector and shows 3.06 times enhancement of photoelectron number in Figure 1d.

Figure 1 illustrates the promise of an external PhC cavity in enhancing the overall detector efficiency. We consider the scintillator material CsI:Na,[41] whose emission spectrum peaks at 410 nm with a full-width-at-half-maximum (FWHM) bandwidth of 120 nm. CsI:Na is widely used in computed tomography (CT).[42] The QE spectrum of PMTs[43] are known to have one of the best overlaps with the emission spectrum of CsI:Na, making the PMT one of the most suitable photodetectors for CsI:Na. However, PMTs do not feature a high QE (around 30% for MCP-PMTs) compared to most APDs. The photodetector we consider in Figure 1 corresponds to the parameters of the APD Hamamatsu-S6429-01[44] with maximum QE 62% at 540 nm and FHWM 64 nm. Although its QE is attractive, the overlap between its QE spectrum and CsI:Na's emission spectrum is relatively small. This forces us to choose between the relatively good spectral overlap of the PMT and the relatively high maximum QE of the APD. Figure 1b-d show that the addition of an external PhC cavity allows us to enjoy the best of both worlds simultaneously, by reshaping the scintillator emission spectrum via the Purcell effect (Figure 1b and 1c). Details on the Purcell factor derivation and photonic band structure calculation are presented in SI Sections I. C and IV respectively. Owing to the Purcell effect, the intrinsic emission spectrum is reshaped to have an improved overlap with the APD QE spectrum. Specifically, the emission peak of CsI:Na is redshifted, as can be seen going from the red to blue curve in Figure 1d. Ultimately, this results in an enhancement of 3.06 times (or > 200%) in photoelectron number and hence detection efficiency, as shown in Figure

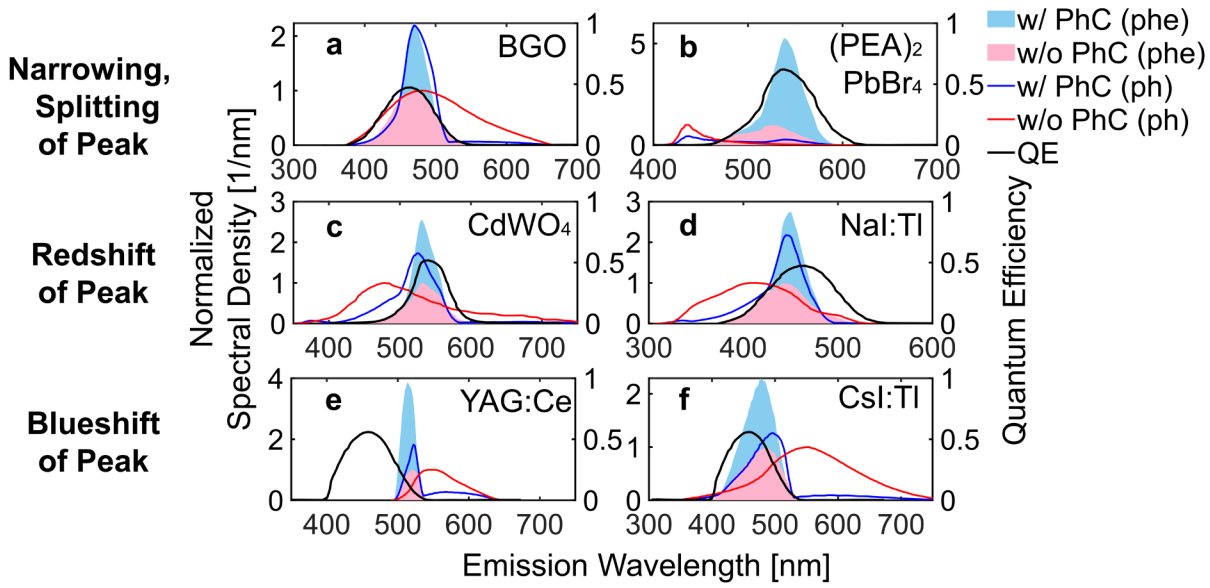

Figure 2. Tailoring the scintillator emission spectrum to achieve greater overlap with the photodetector quantum efficiency (QE) spectrum and hence greater overall photodetector signal. Through the Purcell effect due to the presence of an external photonic crystal (PhC) cavity, the scintillator emission spectral peaks can be narrowed (Figure a), split (Figure b) or shifted (Figure c to f). The PhCs (50 layers on each side) sandwich 1 mm thick scintillators. The name of the scintillator materials used in the simulation are labelled at the top right corners of each panel. The tailored emission spectrum overlaps more with the QE spectrum of the photodetectors, resulting in higher photodetector signal.

1d. The parameters of the PhCs, scintillators, and photodetectors used in the simulation are shown in **Table S1**.

Figure 2 shows the ability of external PhC cavities to reshape the emission spectrum of thick scintillators, thereby achieving enhancing photodetector signal. As examples, the parameters of six leading scintillator materials (activated and self-activated scintillators) and four different types of APDs are used in the simulation.[35, 36, 41] The PhC cavity is composed of alternating layers of dielectric material (refractive index 5) and air. By varying the PhC cavity parameters – which include the refractive indices of constituent layers, layer number, period, and filling factor (the thickness ratio of the higher refractive index material in the PhC) – the emission spectrum can be reshaped in various ways: for instance, to induce a redshift, blueshift, narrowing or splitting of the emission peak. These shaping mechanisms allow us to improve the overlap between the emission spectrum of scintillators and QE spectrum of photodetectors. The narrowing of the peak, for instance, facilitates a better spectral overlap with photodetectors whose QE spectrum have a similarly narrow peak,[45] as in the example shown in Figure 2a. The splitting of the peak is used to improve the photodetector signal in the example shown in Figure 2b. Redshift and blueshift of the emission spectrum are realized in Figure 2c-f. The percentage enhancement in the overall photodetector signal from Figure 2a-f are 32%, 220%, 73%, 63%, 223%, and 90%, respectively.

Figure 3a shows that a larger photodetector signal can generally be obtained with larger PhC refractive index contrast. The PhC is composed of alternating layers of air and dielectric material, whose refractive index varies from 1.5 to 5.0 (shown in the *x* axis of Figure 3a). The number of layers of PhC in each side is set to be 50. The periods and filling factors of PhCs have been optimized for maximum photodetector signal in each case. For comparison, four high efficiency APDs are considered. Our simulation results show that the photodetector signal increases with larger refractive index contrast in the PhC, for all cases, allowing the emission spectrum to be tailored to a larger degree. Figure 3b and 3c explore the impact on photodetector signal by varying periods and filling factors of PhCs for two specific values of refractive index in Figure 3a (circled red points). The photodetector signal enhancement and suppression area are distributed within adjacent fringes. PhC configurations within the enhancement strips would be strongly recommended in future experiment realization.

Figure 4a presents the simulation results for the design of an external PhC cavity-based scintillator device, where the refractive indices used in the PhC layers correspond to those of realistic materials. For the high refractive index component of PhC, we choose TiO_2 as it is a transparent material and has a large refractive index (~2.87)[46] around the emission peak of the scintillator, CsI:Na.[41] For the low refractive index component, we use SiO_2 porous material which can be realized by random SiO_2 nano-rod arrangement.[47] It exhibits a low refractive index around 1.06 in the emission wavelength range. The PhC on each side of the cavity comprises 50 alternating layers of TiO_2 and SiO_2 porous material. In a previous experimental work, PhCs composed of TiO_2 and SiO_2 and have been already proved feasible.[48] Here we replace the SiO_2 film with SiO_2 porous material, which has been shown to be feasibly implemented in PhCs.[47, 49] A possible way to integrate the PhC (TiO_2 + porous SiO_2) and the scintillator CsI:Na could be via eutectic crystals.[50] Eutectic techniques have been proven feasible for the fabrication of PhCs and scintillators.[51-54] Figure 4b shows the overall photodetector signal enhancement as a function of the periodicity and filling factor

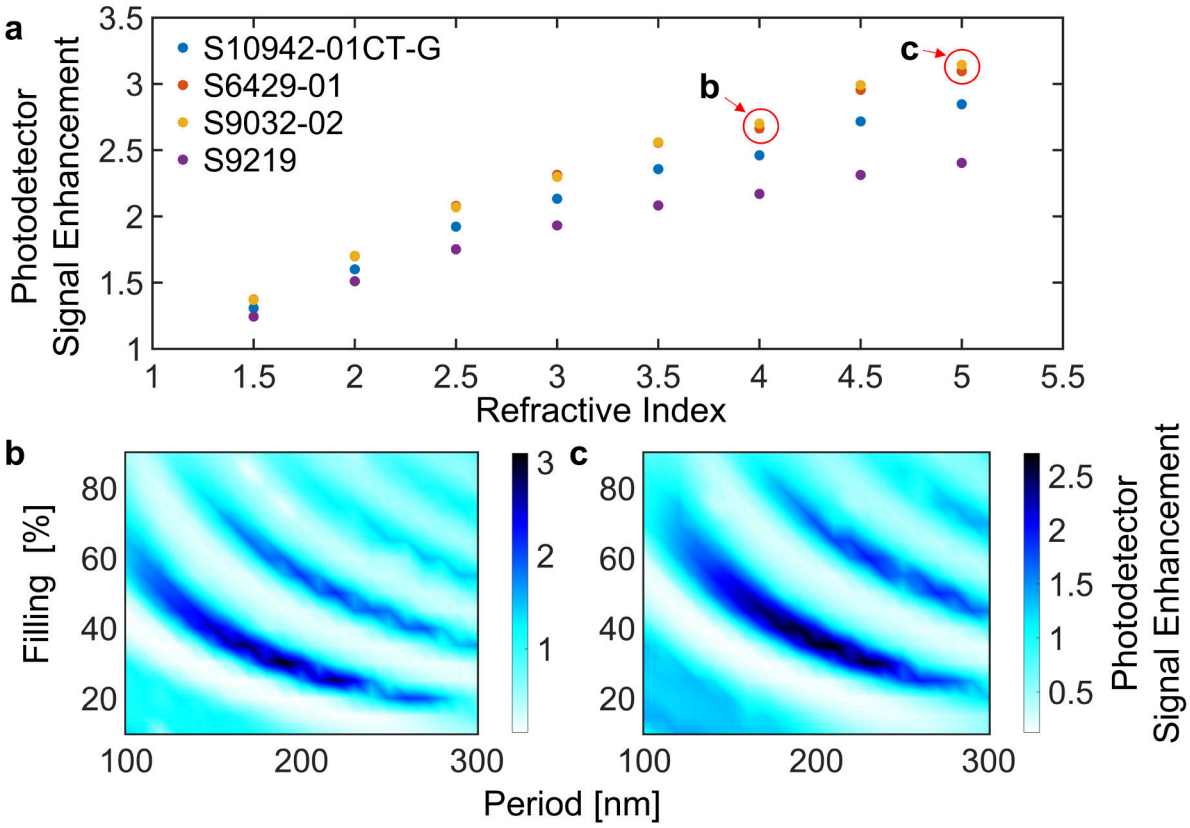

Figure 3. Impact of refractive index contrast on the performance of scintillator system with external photonic crystal (PhC) cavities. The PhCs are composed of alternating layers of dielectric material and air. The PhCs (50 layers on each side) sandwich 1 mm thick CsI:Na. (a) Photodetector signal enhancement vs. refractive index of the dielectric material. The photodetector signal enhancement is defined as the ratio of the photoelectron number detected at the photodetector with the PhC cavity to that without PhC cavity. For each refractive index and photodetector, the results presented correspond to the optimal choice of PhC period and filling factor (the thickness ratio of the higher refractive index material in the PhC). The photodetector signal is improved with increasing refractive index of the dielectric material. The model names of the photodetector (Hamamatsu[44]) used in the simulation are labelled on the left top corner. (b) & (c) Photodetector signal enhancement vs. period and filling factor of PhC for two examples in Figure a (red points in red circles). The maximum enhancement in Figure b and c are 206% and 166%, respectively.

of the PhCs. Figure 4c shows the spectral density of the photons and photoelectrons in the case where maximum enhancement (of 121%, or a factor of 2.21) is achieved. The effect of the PhC cavity is to redshift the scintillator emission peak, resulting in an improved overlap with the photodetector's QE spectrum, and thus an enhanced overall photodetector signal. Other high refractive index materials we could consider for the PhC includes SiC, Diamond and $SrTiO_3$ – these scenarios are analyzed in SI Section V. Besides SiO_2, the low refractive index material could also be replaced by other transparent porous materials.[55-59]

In practice, at least slight fabrication errors may occur when manufacturing the nanofilm layers of the PhC structure. To ensure stable performance of PhC cavity-based scintillators system in experiments, it is crucial to consider the influence of fabrication accuracy on the scintillator photodetector signal. We model the thickness of dielectric layer of PhC as a random variable governed by a Gaussian distribution. **Figure 5** explores the impact of the standard deviation (SD) of layer thickness and the layer number of PhC on scintillation performance. The numerical results show that the performance of the scintillator worsens when both the layer number and SD increase. More details of the impact of fabrication errors on the scintillation performance can be found on the SI Section VI.

Discussion

One-dimensional (1D) PhC structures are made of periodically alternating layers. Featuring periods typically of several hundreds of nanometers, 1D PhCs have shown the ability to tailor visible light emission, such as that generated from free electron radiation.[60-65] Our use of a 1D model makes our theory valid only for devices whose transverse dimensions are much larger than their thickness -- which include many types of large-area detectors.[28] These large-area detectors are widely used in many scintillation field, including medical X-ray imaging, security scanning, dark matter detection, and neutrino detection.[6-11, 29, 30] In this work, The Purcell effect enabled by external PhC cavities allows us to mold the scintillator emission pattern beyond what is possible by just using external structures as reflective/transmissive media. This ultimately allows the overall photodetector signal to be enhanced, by molding the emission spectrum to have a greater overlap with the QE spectrum of the corresponding photodetectors. Generally, most standard scintillator materials have a specific emission spectrum,[31, 34] which means the choices for photodetectors

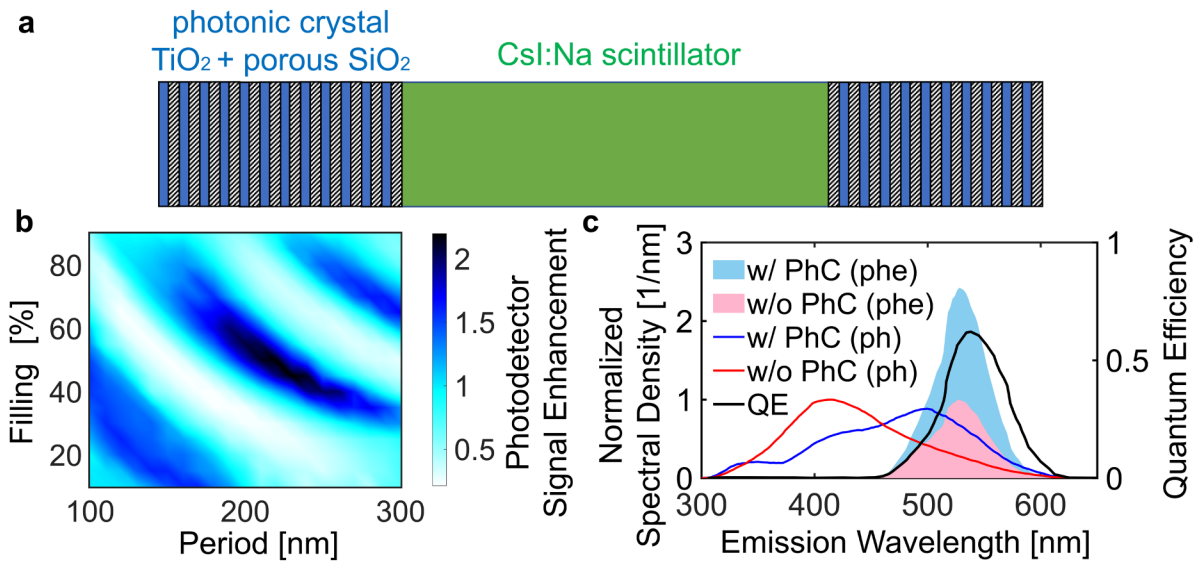

Figure 4. External photonic crystal (PhC) cavity-enhanced scintillator system using actual materials. (a) Schematic diagram of CsI:Na scintillator with a PhC cavity (TiO_2 + porous SiO_2). The TiO_2/SiO_2 PhCs have been shown to be feasible in previous work.[48] Here, we replace SiO_2 film with SiO_2 porous material so as to achieve a low refractive index (1.06)[47] for the SiO_2 layer. SiO_2 porous material can be realized by random SiO2 nano-rod arrangement. (b) Photodetector signal enhancement vs. period & filling factor of photonic crystal. (c) Spectral density of photons (ph) & photoelectrons (phe) with optimized configuration of PhC cavity (TiO_2 + porous SiO_2). The emission spectrum is shifted to longer wavelength to match the quantum efficiency (QE) spectrum of the photodetector. The enhancement of the overall photodetector signal is 121%.

are very limited.[66] For example, Microchannel plate PMTs (MCP-PMTs)[67] are widely used for scintillators with emission wavelengths around 350 to 450 nm, e.g., CsI:Na. But the QE of MCP-PMT is moderate at around 30% due to its high working frequency and broad band response. On the contrary, photodetectors with high QE (e.g., APDs[68, 69]) often work in a relatively long wavelength range (over 500 nm) and small bandwidth, which cannot achieve high photodetector signal for most scintillators because of the lack of overlap between emission spectrum and QE spectrum. This often forces users to choose between the relatively good spectral overlap of PMTs, versus the relatively good peak QE efficiency of APDs. As presented in this work, external PhC cavities can be used to achieve the best of both worlds, by tailoring the emission spectrum of scintillators so that APDs can be used with a relatively good spectral overlap. This allows for more versatility in choosing combinations of photodetectors and scintillator materials, and also higher resulting photodetector signal.

The tailoring mechanism of Purcell factor by PhC cavities is different from the situation where scintillator itself is fabricated into a 1D PhC. In the latter case, the enhancement of decay rate comes from the dipoles located close to the surface. It requires the filling factor of scintillator to be small enough to enable more near-surface dipoles. In the PhC cavity-based scintillator system, the Purcell factor is tailored by the photonic band structure construed by the external PhC cavity. By implementing the high refractive contrast PhCs, we could tailor the Purcell factor and thus redistribute the emission spectrum.

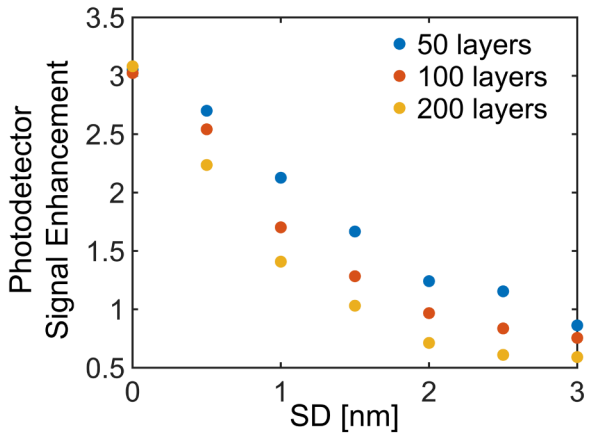

Figure 5. Impact of the standard deviation (SD) of every dielectric layer of photonic crystal (PhC) on the scintillator photodetector signal enhancement. The PhC is composed of alternating layers of dielectric material (refractive index 5) and air. The scintillator used is a 1mm thick CsI:Na. The layer number (on each side) varies from 50 to 200. With the increase of the deviation from ideal PhC, the randomness increases and the photodetector signal drops. With the increase of the layer number, the influence of the SD increases. The results are based on the average of 10 runs.

Although naturally occurring materials cannot push a higher limit, novel research in nanostructures can be applied to further enlarge the refractive index contrast of PhC. The high refractive index materials can be achieved by metamaterials[70-72], e.g., stacked cut-wire plasmonic structures (n~7)[72], metal film with periodic slits (n~16)[70], etc. The low refractive index materials can be achieved by near-zero-index (NZI) materials[73-77], an example of which

can be constructed by all-dielectric zero-index optical metamaterial[75]. PhCs composed of those novel structures are promising to achieve a higher photodetector signal. Furthermore, to avoid the loss due to the photon absorption of PhC, it is recommended to pick all dielectric design of metamaterials and NZI materials.[71, 75]

The enhancements possible with 1D external PhC cavities also raise the exciting prospects of 2D/3D external PhC cavities, including even more complicated nanostructures that might be realized using 3D printers. Higher dimension PhCs could form more complicated photonic band structures[28, 78-80] and lead to even more versatility in tailoring the emission spectrum. Apart from periodic crystal, quasicrystals[81, 82] and chirped crystals[83] are also promising candidates for different photonic band structures and could realize different ways to reshape the emission spectrum. Furthermore, it is intriguing to consider real-time tuning of scintillator emission through real-time tuning of the external PhC cavities, which have been shown to be tailorable via structural/chemical tuning[84] or even by electric signals when graphene is introduced as a coating[85].

While we mainly focus on the spectral distribution of photons and photoelectrons, our theoretical framework can also handle the angular distribution analysis. Similar with wavelength, the angular distribution of the Purcell factor can also be tailored by the photonic band structure constructed by photonic crystal and results in the tailoring of angular distribution of the photons. It would be meaningful when some photodetectors have angular distribution of QE.[86] Considering the angular overlap of the photon emission and photodetector QE, the total photoelectron number can be further enhanced by accumulating the photons in certain emission angles where photodetectors show a higher QE.

As is shown in Figure 5, the performance of the scintillator benefits from the lower layer number and smaller SD of the individual dielectric layer thickness. This in fact highlights two advantages of our external 1D PhC cavity design compared to an alternative scheme where the scintillator itself is fabricated into a 1D PhC, and whose performance similarly deteriorates with number of layers.[25] Firstly, if scintillator itself is fabricated into a 1D PhC, the layer number should be large so as to absorb incident high energy particles.[25] However, we do not need PhCs with a large number of layers in external 1D PhC cavity because the role to absorb incident high energy particles is the thick scintillator in the middle. The PhC cavity is only to form a suitable band structure to tailor the emission spectrum via the Purcell effect. Therefore, external PhC cavity-based scintillator system will be less influenced because of the less layer number needed. Secondly, it may be impractical to convert the scintillator material itself into a 1D PhC when the scintillator material has to be very thick, for example for neutrino detectors, as this would result in large number of scintillator layers that negatively impacts the fabrication sensitivity and worsens the physical stability.[8, 87] On the other hand, less layers would benefit the scintillator performance in another perspective. The high energy particles can sometimes be absorbed by the dielectric materials, not by the scintillators, which could cause energy loss. The decrease of layer number in external PhC cavity-based scintillator system can reduce this loss. Based on the analysis of fabrication errors, it will provide reference for the future experimental verification and applications.

To summarize, we have shown numerically that external PhC cavities can tailor the emission spectra of thick scintillators, enhancing the photodetector signal by over 200% due to the improved overlap between the scintillator's emission spectrum and the photodetector's QE spectrum. We have shown that the choice of external PhC geometry and material can be used to shape the emission spectrum in various ways, including shifting, narrowing and splitting of the emission peaks. The presence of the external PhC cavity thus makes each scintillator material much more versatile, allowing it to be compatible with a wider range of available photodetectors. Besides, considering the experimental verification and further applications, we demonstrate that with the increase of the fabrication error of the layer thickness and the increase of the layer number, the photodetector signal declines. Therefore, a relatively low layer number enough to form a suitable band structure is suggested, which also reduces the absorption of high energy particles by the non-scintillator material. The external PhC cavity-based scintillator design is especially beneficial to applications that need a large area or large thickness scintillator detector, e.g., PET scanners and neutrino detectors because the atomic structure and geometrical structure of the scintillator do not need to be modified in this system. Other applications including X-ray imaging and high energy particle detection can also benefit from higher scintillator photodetector signal and lower incident radiation dose. Furthermore, in terms of fast response applications such as PET, the increase in photodetector signal will improve timing resolution significantly.

Methods

A general framework for 1D external photonic crystal cavity-enhanced scintillators: In the scintillation process, numerous dipoles are produced inside the crystal and the Purcell factor of the dipole is defined using $\gamma(\boldsymbol{r}, \omega, \theta, \sigma)$,[25] where $\boldsymbol{r}$ denotes the position of the dipoles and ω, θ, σ denote the emission angular frequency, angle, polarization, respectively. The emission rate of a dipole $\Gamma(\boldsymbol{r}, \omega, \theta, \sigma) = \Gamma_0(\omega, \sigma)\gamma(\boldsymbol{r}, \omega, \theta, \sigma)$ represents the number of photons produced by the dipoles in a certain position per unit time with a certain emission wavelength, angle, and polarization. $\Gamma_0(\omega, \sigma)$ denotes the emission rate of a dipole in vacuum with a certain wavelength and emission polarization. The effective decay time for a dipole located at a certain position $\boldsymbol{r}$ could be written as

$$\tau_{eff}(\boldsymbol{r}) = \frac{1}{\Gamma_{eff}(\boldsymbol{r})} = \frac{1}{\int d\omega Y(\omega) \int_0^{\frac{\pi}{2}} d\theta \, sin\,\theta \sum_\sigma \Gamma(\boldsymbol{r}, \omega, \theta, \sigma)} \quad (1)$$

where $Y(\omega)$ is the intrinsic emission spectrum of a dipole which is normalized by $\int Y(\omega)d\omega = 1$ (see SI Section I. B). In a 1D layered system, position could be denoted by z. The total number of the photons produced by dipoles located within dz area:

$$N_p(z)dz = \frac{\Gamma_{eff}^T(z)}{\Gamma_{eff}(z)}\{N_{d,0}G(z)dz\} \quad (2)$$

$$\Gamma_{eff}^{T}(z) = \int d\omega Y(\omega) \int_0^{\frac{\pi}{2}} d\theta \sin\theta \sum_{\sigma} T(z,\omega,\theta,\sigma)\Gamma(z,\omega,\theta,\sigma) \quad (3)$$

where $T(z,\omega,\theta,\sigma)$ denotes the transmission coefficient of photons produced at position z. $N_{d,0}$ denotes the total number of radiative dipole emitters inside the scintillator. $G(z)$ denotes the spatial distribution of the dipole emitters. In this work, we take an exponential decay of the dipole density with the depth from the surface. Therefore, dipole distribution function could be written as:

$$G(z) = \frac{\frac{1}{\kappa} e^{-\frac{z}{\kappa}}}{1 - e^{-\frac{L}{\kappa}}} \quad (4)$$

where L is the total length of the scintillator material, κ is the linear attenuation coefficient of incident high energy photons for the scintillator material. The data of linear attenuation coefficient in this work is from NIST database.[88] The results under another dipole distribution type, uniform distribution, is presented in Figure S6.

The number of photons detected over time combines the influence of total photon number, the decay rate and the dipole position:

$$n_{tot}(t) = \int_0^L \{N_p(z)dz\} \left[1 - e^{-\left(\frac{1}{\tau_{eff}(z)}\right)t}\right] \quad (5)$$

After the photons pass through a photodetector with a quantum efficiency $QE(\omega)$ varying with wavelength, the total number of photoelectrons at the photodetector produced by dipoles located within dz area could be written as

$$N_e(z)dz = \frac{\Gamma_{eff}^{T,e}(z)}{\Gamma_{eff}(z)} \{N_{d,0} G(z) dz\} \quad (6)$$

$$\Gamma_{eff}^{T,e}(z) = \int d\omega Y(\omega) QE(\omega) \int_0^{\frac{\pi}{2}} d\theta \sin\theta \sum_{\sigma} T(z,\omega,\theta,\sigma)\Gamma(z,\omega,\theta,\sigma) \quad (7)$$

The enhancement of the decay rate, the detected photon number, and the detected photoelectron number for a dipole at a certain position z could be written as $\tau_{eff,Bulk}(z)/\tau_{eff,PhC}(z)$, $N_{p,PhC}(z)/N_{p,Bulk}(z)$, and $N_{e,PhC}(z)/N_{e,Bulk}(z)$, where $\tau_{eff,Bulk}(z)$, $N_{p,Bulk}(z)$, and $N_{e,Bulk}(z)$ denote the decay time, detected photon number, and detected photoelectron number for a dipole located at a certain position z in a thick single-crystal (bulk) scintillator. More details can be found in SI Section I.

Influence of dipole distribution on the scintillator performance: See SI Section II for details.

Influence of the loss of the scintillator on the Purcell factor and scintillator performance: See SI Section III for details.

Photonic band structure calculation of one-dimensional photonic crystal: See SI Section IV for details.

Designs with realistic materials: See SI Section V for details.

The influence of the fabrication error on the scintillation performance: See SI Section VI for details.

Quantum efficiency of the photodetectors: See SI Section VII for details.

ASSOCIATED CONTENT

The Supporting Information is available free of charge via the Internet at http://pubs.acs.org.

Theory of scintillation processes in layered medium; Influence of dipole distribution on the scintillator performance; Influence of the loss of scintillator material on the Purcell factor and scintillator performance; Photonic band structure calculation of one-dimensional photonic crystal based on plane wave expansion; Designs with realistic materials; The influence of the fabrication error on the scintillation performance; Quantum efficiency of the photodetectors. (PDF)

AUTHOR INFORMATION

Corresponding Author

*Liang Jie Wong - School of Electrical and Electronic Engineering, Nanyang Technological University, 50 Nanyang Avenue, Singapore 639798, Singapore; CNRS-International-NTU-THALES Research Alliance (CINTRA), Nanyang Technological University, 50 Nanyang Drive, 637553, Singapore; Email: liangjie.wong@ntu.edu.sg

*Muhammad D. Birowosuto - Łukasiewicz Research Network-PORT Polish Center for Technology Development, Stabłowicka 147, 54-066 Wrocław, Poland; Email: muhammad.birowosuto@prasetiyamulya.ac.id

Author Contributions

Author contributions: Wenzheng Ye led the project and analyzed the data. Wenzheng Ye developed the theory and performed the simulations with the help of Liang Jie Wong. Wenzheng Ye, Gregory Bizarri, Muhammad D. Birowosuto, and Liang Jie Wong wrote the paper. Liang Jie Wong and Muhammad D. Birowosuto conceived the idea and supervised the project. **Data Available:** All data needed to evaluate the conclusions in the paper are present in the manuscript and the Supporting Information. Additional data that support the plots within this paper are available from the corresponding authors upon reasonable request.

Funding Sources

L.J.W. acknowledges the Nanyang Assistant Professorship Start-up Grant.

Notes

The authors declare no competing interests.

ACKNOWLEDGMENT

The authors would like to thank Dominik Kowal for helpful discussions.

REFERENCES

(1) Gundacker, S.; Turtos, R. M.; Auffray, E.; Paganoni, M.; Lecoq, P. High-frequency SiPM readout advances measured coincidence time resolution limits in TOF-PET. *Physics in Medicine & Biology* **2019**, *64* (5), 055012.

(2) Moszyński, M.; Szawlowski, M.; Kapusta, M.; Balcerzyk, M. Large area avalanche photodiodes in scintillation and X-rays detection. *Nuclear Instruments and Methods in Physics Research Sec-*

tion A: Accelerators, Spectrometers, Detectors and Associated Equipment **2002**, *485* (3), 504-521.

(3) Schaart, D. R. Physics and technology of time-of-flight PET detectors. *Physics in Medicine & Biology* **2021**, *66* (9), 09TR01.

(4) Schaart, D. R.; van Dam, H. T.; Seifert, S.; Vinke, R.; Dendooven, P.; Löhner, H.; Beekman, F. J. A novel, SiPM-array-based, monolithic scintillator detector for PET. *Physics in Medicine & Biology* **2009**, *54* (11), 3501.

(5) Van Eijk, C. W. Inorganic scintillators in medical imaging. *Physics in Medicine & Biology* **2002**, *47* (8), R85.

(6) Glodo, J.; Wang, Y.; Shawgo, R.; Brecher, C.; Hawrami, R. H.; Tower, J.; Shah, K. S. New developments in scintillators for security applications. *Physics Procedia* **2017**, *90*, 285-290.

(7) Cecil, R.; Anderson, B.; Madey, R. Improved predections of neutron detection efficiency for hydrocarbon scintillators from 1 MeV to about 300 MeV. *Nuclear Instruments and Methods* **1979**, *161* (3), 439-447.

(8) Eguchi, K.; Enomoto, S.; Furuno, K.; Ikeda, H.; Ikeda, K.; Inoue, K.; Ishihara, K.; Iwamoto, T.; Kawashima, T.; Kishimoto, Y.; et al. High sensitivity search for nu;e's from the sun and other sources at KamLAND. *Physical Review Letters* **2004**, *92* (7), 071301. DOI: 10.1103/PhysRevLett.92.071301.

(9) Collaboration, C.-. An experiment to search for dark-matter interactions using sodium iodide detectors. *Nature* **2018**, *564* (7734), 83-86. DOI: 10.1038/s41586-018-0739-1.

(10) Athanassopoulos, C.; Auerbach, L.; Bauer, D.; Bolton, R.; Burman, R.; Cohen, I.; Caldwell, D.; Dieterle, B.; Donahue, J.; Eisner, A. The Liquid scintillator neutrino detector and LAMPF neutrino source. *Nuclear Instruments and Methods in Physics Research Section A: Accelerators, Spectrometers, Detectors and Associated Equipment* **1997**, *388* (1-2), 149-172.

(11) Araki, T.; Eguchi, K.; Enomoto, S.; Furuno, K.; Ichimura, K.; Ikeda, H.; Inoue, K.; Ishihara, K.; Iwamoto, T.; Kawashima, T. Measurement of neutrino oscillation with KamLAND: Evidence of spectral distortion. *Physical Review Letters* **2005**, *94* (8), 081801.

(12) Sengupta, D.; Miller, S.; Marton, Z.; Chin, F.; Nagarkar, V.; Pratx, G. Bright Lu2O3 :Eu Thin-Film Scintillators for High-Resolution Radioluminescence Microscopy. *Advanced Healthcare Materials* **2015**, *4* (14), 2064-2070. DOI: 10.1002/adhm.201500372.

(13) Fasoli, M.; Vedda, A.; Nikl, M.; Jiang, C.; Uberuaga, B.; Andersson, D.; McClellan, K.; Stanek, C. Band-gap engineering for removing shallow traps in rare-earth Lu 3 Al 5 O 12 garnet scintillators using Ga 3+ doping. *Physical Review B* **2011**, *84* (8), 081102.

(14) Chen, Q.; Wu, J.; Ou, X.; Huang, B.; Almutlaq, J.; Zhumekenov, A. A.; Guan, X.; Han, S.; Liang, L.; Yi, Z. All-inorganic perovskite nanocrystal scintillators. *Nature* **2018**, *561* (7721), 88-93.

(15) Maddalena, F.; Tjahjana, L.; Xie, A.; Arramel; Zeng, S.; Wang, H.; Coquet, P.; Drozdowski, W.; Dujardin, C.; Dang, C.; et al. Inorganic, Organic, and Perovskite Halides with Nanotechnology for High–Light Yield X- and γ-ray Scintillators. *Crystals* **2019**, *9* (2). DOI: 10.3390/cryst9020088.

(16) Kakavelakis, G.; Gedda, M.; Panagiotopoulos, A.; Kymakis, E.; Anthopoulos, T. D.; Petridis, K. Metal Halide Perovskites for High-Energy Radiation Detection. *Advanced Science* **2020**, *7* (22), 2002098. DOI: 10.1002/advs.202002098.

(17) Birowosuto, M. D.; Cortecchia, D.; Drozdowski, W.; Brylew, K.; Lachmanski, W.; Bruno, A.; Soci, C. X-ray Scintillation in Lead Halide Perovskite Crystals. *Scientific Reports* **2016**, *6*, 37254. DOI: 10.1038/srep37254.

(18) Zhang, H.; Yang, Z.; Zhou, M.; Zhao, L.; Jiang, T.; Yang, H.; Yu, X.; Qiu, J.; Yang, Y.; Xu, X. Reproducible X‐ray Imaging with a Perovskite Nanocrystal Scintillator Embedded in a Transparent Amorphous Network Structure. *Advanced Materials* **2021**, *33* (40), 2102529.

(19) Ma, W.; Jiang, T.; Yang, Z.; Zhang, H.; Su, Y.; Chen, Z.; Chen, X.; Ma, Y.; Zhu, W.; Yu, X. Highly Resolved and Robust Dynamic X‐Ray Imaging Using Perovskite Glass‐Ceramic Scintillator with Reduced Light Scattering. *Advanced Science* **2021**, *8* (15), 2003728.

(20) Tjahjana, L.; Lee, K.; Chin, X. Y.; Tobing, L. Y. M.; Adhyaksa, G. W. P.; Zhang, D. H.; Birowosuto, M. D.; Wang, H. Controlling Spontaneous Emission from Perovskite Nanocrystals with Metal–Emitter–Metal Nanostructures. *Crystals* **2020**, *11* (1). DOI: 10.3390/cryst11010001.

(21) Salomoni, M.; Pots, R.; Auffray, E.; Lecoq, P. Enhancing Light Extraction of Inorganic Scintillators Using Photonic Crystals. *Crystals* **2018**, *8* (2). DOI: 10.3390/cryst8020078.

(22) Zhu, Z.; Wu, S.; Xue, C.; Zhao, J.; Wang, L.; Wu, Y.; Liu, B.; Cheng, C.; Gu, M.; Chen, H. Enhanced light extraction of scintillator using large-area photonic crystal structures fabricated by soft-X-ray interference lithography. *Applied Physics Letters* **2015**, *106* (24), 241901.

(23) Kronberger, M.; Auffray, E.; Lecoq, P. Probing the concepts of photonic crystals on scintillating materials. *IEEE Transactions on Nuclear Science* **2008**, *55* (3), 1102-1106.

(24) Novotny, L.; Hecht, B. *Principles of nano-optics*; Cambridge university press, 2012.

(25) Kurman, Y.; Shultzman, A.; Segal, O.; Pick, A.; Kaminer, I. Photonic-crystal scintillators: Molding the flow of light to enhance X-ray and γ-ray detection. *Physical Review Letters* **2020**, *125* (4), 040801.

(26) Roques-Carmes, C.; Rivera, N.; Ghorashi, A.; Kooi, S. E.; Yang, Y.; Lin, Z.; Beroz, J.; Massuda, A.; Sloan, J.; Romeo, N.; et al. A framework for scintillation in nanophotonics. *Science* **2022**, *375* (6583), eabm9293. DOI: 10.1126/science.abm9293.

(27) Lahav, N.; Kurman, Y.; Schuetz, R.; Lifshits, A.; Zaken, S.; Be'er, O.; Bekenstein, Y.; Kaminer, I. Purcell enhancement of X-ray scintillation. In *CLEO: Science and Innovations*, 2022; Optica Publishing Group: p SM3K. 7.

(28) Joannopoulos, J. D.; Johnson, S. G.; Winn, J. N.; Meade, R. D. Molding the flow of light. *Princeton Univ. Press, Princeton, NJ [ua]* **2008**.

(29) Fushimi, K.; Nakayama, S.; Orito, R.; Sugawara, R.; Awatani, Y.; Ejiri, H.; Shima, T.; Hazama, R.; Inoue, K.; Ikeda, H. PICO-LON dark matter search. In *Journal of Physics: Conference Series*, 2013; IOP Publishing: Vol. 469, p 012011.

(30) Nagarkar, V.; Gupta, T.; Miller, S.; Klugerman, Y.; Squillante, M.; Entine, G. Structured CsI (Tl) scintillators for X-ray imaging applications. *IEEE transactions on nuclear science* **1998**, *45* (3), 492-496.

(31) Gektin, A.; Korzhik, M. *Inorganic scintillators for detector systems*; Springer, 2017.

(32) Van Eijk, C. W. Inorganic-scintillator development. *Nuclear Instruments and Methods in Physics Research Section A: Accelerators, Spectrometers, Detectors and Associated Equipment* **2001**, *460* (1), 1-14.

(33) Nikl, M. Scintillation detectors for x-rays. *Measurement Science and Technology* **2006**, *17* (4), R37-R54. DOI: 10.1088/0957-0233/17/4/r01.

(34) Knoll, G. F. *Radiation detection and measurement*; John Wiley & Sons, 2010.

(35) Burachas, S. P.; Danevich, F.; Georgadze, A. S.; Klapdor-Kleingrothaus, H.; Kobychev, V.; Kropivyansky, B.; Kuts, V.; Muller, A.; Muzalevsky, V.; Nikolaiko, A. Large volume CdWO4 crystal scintillators. *Nuclear Instruments and Methods in Physics Research Section A: Accelerators, Spectrometers, Detectors and Associated Equipment* **1996**, *369* (1), 164-168.

(36) Weber, S.; Christ, D.; Kurzeja, M.; Engels, R.; Kemmerling, G.; Halling, H. Comparison of LuYAP, LSO, and BGO as scintillators for high resolution PET detectors. *IEEE Transactions on Nuclear Science* **2003**, *50* (5), 1370-1372.

(37) Birowosuto, M.; Dorenbos, P. Novel γ‐ and X‐ray scintillator research: on the emission wavelength, light yield and time response of Ce3+ doped halide scintillators. *Physica Status Solidi (a)* **2009**, *206* (1), 9-20.

(38) Chewpraditkul, W.; Swiderski, L.; Moszynski, M.; Szczesniak, T.; Syntfeld-Kazuch, A.; Wanarak, C.; Limsuwan, P. Scintillation properties of LuAG: Ce, YAG: Ce and LYSO: Ce crystals for gamma-ray detection. *IEEE Transactions on Nuclear Science* **2009**, *56* (6), 3800-3805.

(39) Dorenbos, P. The 5d level positions of the trivalent lanthanides in inorganic compounds. *Journal of Luminescence* **2000**, *91* (3-4), 155-176.

(40) Weber, M. Scintillation: mechanisms and new crystals. *Nuclear Instruments and Methods in Physics Research Section A: Accelerators, Spectrometers, Detectors and Associated Equipment* **2004**, *527* (1-2), 9-14.

(41) Aitken, D.; Beron, B.; Yenicay, G.; Zulliger, H. The fluorescent response of NaI (Tl), CsI (Tl), CsI (Na) and CaF2 (Eu) to X-rays and low energy gamma rays. *IEEE Transactions on Nuclear Science* **1967**, *14* (1), 468-477.

(42) Sánchez, F.; Orero, A.; Soriano, A.; Correcher, C.; Conde, P.; González, A.; Hernández, L.; Moliner, L.; Rodríguez‐Alvarez, M. J.; Vidal, L. ALBIRA: a small animal PET/SPECT/CT imaging system. *Medical Physics* **2013**, *40* (5), 051906.

(43) David, S.; Georgiou, M.; Fysikopoulos, E.; Belcari, N.; Loudos, G. Imaging performance of silicon photomultipliers coupled to BGO and CsI: Na arrays. *Journal of Instrumentation* **2013**, *8* (12), P12008.

(44) *Hamamatsu Photonics Home Page*. https://www.hamamatsu.com/ (accessed 2022-09-02).

(45) Xue, J.; Zhu, Z.; Xu, X.; Gu, Y.; Wang, S.; Xu, L.; Zou, Y.; Song, J.; Zeng, H.; Chen, Q. Narrowband perovskite photodetector-based image array for potential application in artificial vision. *Nano Letters* **2018**, *18* (12), 7628-7634.

(46) DeVore, J. R. Refractive indices of rutile and sphalerite. *JOSA* **1951**, *41* (6), 416-419.

(47) Schubert, E. F.; Kim, J. K.; Xi, J. Q. Low-refractive-index materials: A new class of optical thin-film materials. *Physica Status Solidi (b)* **2007**, *244* (8), 3002-3008. DOI: 10.1002/pssb.200675603.

(48) Ghazzal, M. N.; Deparis, O.; De Coninck, J.; Gaigneaux, E. M. Tailored refractive index of inorganic mesoporous mixed-oxide Bragg stacks with bio-inspired hygrochromic optical properties. *Journal of Materials Chemistry C* **2013**, *1* (39), 6202-6209.

(49) Calvo, M. E.; Colodrero, S.; Hidalgo, N.; Lozano, G.; López-López, C.; Sánchez-Sobrado, O.; Míguez, H. Porous one dimensional photonic crystals: novel multifunctional materials for environmental and energy applications. *Energy & Environmental Science* **2011**, *4* (12). DOI: 10.1039/c1ee02081a.

(50) Rastogi, R.; Rastogi, V. Mechanism of eutectic crystallization. II. *Journal of Crystal Growth* **1969**, *5* (5), 345-353.

(51) Choi, J.; Kulkarni, A. A.; Hanson, E.; Bacon‐Brown, D.; Thornton, K.; Braun, P. V. Processing‐Dependent Microstructure of AgCl–CsAgCl2 Eutectic Photonic Crystals. *Advanced Optical Materials* **2018**, *6* (14), 1701316.

(52) Kim, J.; Aagesen, L. K.; Choi, J. H.; Choi, J.; Kim, H. S.; Liu, J.; Cho, C. R.; Kang, J. G.; Ramazani, A.; Thornton, K. Template‐Directed Directionally Solidified 3D Mesostructured AgCl–KCl Eutectic Photonic Crystals. *Advanced Materials* **2015**, *27* (31), 4551-4559.

(53) Wu, Y.; Lukosi, E. D.; Zhuravleva, M.; Lindsey, A. C.; Melcher, C. L. A novel LiCl–BaCl2: Eu2+ eutectic scintillator for thermal neutron detection. *Nuclear Instruments and Methods in Physics Research Section A: Accelerators, Spectrometers, Detectors and Associated Equipment* **2015**, *797*, 319-323.

(54) Yanagida, T.; Fujimoto, Y.; Fukuda, K.; Kawaguchi, N.; Watanabe, K.; Yamazaki, A.; Uritani, A.; Chani, V. Ce-doped LiF–SrF2 eutectic scintillators for thermal neutron detection produced at different solidification rates. *Optical Materials* **2013**, *35* (7), 1449-1454.

(55) Bennett, T. D.; Coudert, F. X.; James, S. L.; Cooper, A. I. The changing state of porous materials. *Nature Materials* **2021**, *20* (9), 1179-1187. DOI: 10.1038/s41563-021-00957-w.

(56) Frohnhoff, S.; Berger, M. G. Porous silicon superlattices. *Advanced Materials* **1994**, *6* (12), 963-965.

(57) Falcaro, P.; Malfatti, L.; Kidchob, T.; Giannini, G.; Falqui, A.; Casula, M. F.; Amenitsch, H.; Marmiroli, B.; Grenci, G.; Innocenzi, P. Hierarchical porous silica films with ultralow refractive index. *Chemistry of Materials* **2009**, *21* (10), 2055-2061.

(58) Khardani, M.; Bouaïcha, M.; Bessaïs, B. Bruggeman effective medium approach for modelling optical properties of porous silicon: comparison with experiment. *Physica Status Solidi c* **2007**, *4* (6), 1986-1990.

(59) Tao, C.; Zou, X.; Du, K.; Zhang, L.; Yan, H.; Yuan, X. Ultralow-refractive-index optical thin films built from shape-tunable hollow silica nanomaterials. *Optics Letters* **2018**, *43* (8), 1802-1805.

(60) Hu, H.; Lin, X.; Luo, Y. Free-Electron Radiation Engineering via Structured Environments. *Progress In Electromagnetics Research* **2021**, *171*, 75-88.

(61) Lin, X.; Easo, S.; Shen, Y.; Chen, H.; Zhang, B.; Joannopoulos, J. D.; Soljačić, M.; Kaminer, I. Controlling Cherenkov angles with resonance transition radiation. *Nature Physics* **2018**, *14* (8), 816-821.

(62) Lin, X.; Hu, H.; Easo, S.; Yang, Y.; Shen, Y.; Yin, K.; Blago, M. P.; Kaminer, I.; Zhang, B.; Chen, H. A Brewster route to Cherenkov detectors. *Nature Communications* **2021**, *12* (1), 1-7.

(63) Huang, S.; Duan, R.; Pramanik, N.; Boothroyd, C.; Liu, Z.; Wong, L. J. Enhanced Versatility of Table‐Top X‐Rays from Van der Waals Structures. *Advanced Science* **2022**, 2105401.

(64) Tan, Y. J.; Pitchappa, P.; Wang, N.; Singh, R.; Wong, L. J. Space‐Time Wave Packets from Smith‐Purcell Radiation. *Advanced Science* **2021**, *8* (22), 2100925.

(65) Wong, L. J.; Kaminer, I.; Ilic, O.; Joannopoulos, J. D.; Soljačić, M. Towards graphene plasmon-based free-electron infrared to X-ray sources. *Nature Photonics* **2016**, *10* (1), 46-52.

(66) Sakai, E. Recent measurements on scintillator-photodetector systems. *IEEE Transactions on Nuclear Science* **1987**, *34* (1), 418-422.

(67) Wang, Y.; Qian, S.; Zhao, T.; Tian, J.; Li, H.; Cao, J.; Xu, X.; Wang, X.; Liu, S.; Liu, H. A new design of large area MCP-PMT for the next generation neutrino experiment. *Nuclear Instruments and Methods in Physics Research Section A: Accelerators, Spectrometers, Detectors and Associated Equipment* **2012**, *695*, 113-117.

(68) Emmons, R. Avalanche‐photodiode frequency response. *Journal of Applied Physics* **1967**, *38* (9), 3705-3714.

(69) Kardynał, B.; Yuan, Z.; Shields, A. An avalanche‐photodiode-based photon-number-resolving detector. *Nature Photonics* **2008**, *2* (7), 425-428.

(70) Shen, J.-T.; Catrysse, P. B.; Fan, S. Mechanism for designing metallic metamaterials with a high index of refraction. *Physical Review Letters* **2005**, *94* (19), 197401.

(71) Krishnamoorthy, H.; Adamo, G.; Yin, J.; Savinov, V.; Zheludev, N.; Soci, C. Infrared dielectric metamaterials from high refractive index chalcogenides. *Nature Communications* **2020**, *11* (1), 1-6.

(72) Wei, X.; Shi, H.; Dong, X.; Lu, Y.; Du, C. A high refractive index metamaterial at visible frequencies formed by stacked cut-wire plasmonic structures. *Applied Physics Letters* **2010**, *97* (1), 011904.

(73) Kinsey, N.; DeVault, C.; Boltasseva, A.; Shalaev, V. M. Near-zero-index materials for photonics. *Nature Reviews Materials* **2019**, *4* (12), 742-760. DOI: 10.1038/s41578-019-0133-0.

(74) Liberal, I.; Engheta, N. Near-zero refractive index photonics. *Nature Photonics* **2017**, *11* (3), 149-158. DOI: 10.1038/nphoton.2017.13.

(75) Moitra, P.; Yang, Y.; Anderson, Z.; Kravchenko, I. I.; Briggs, D. P.; Valentine, J. Realization of an all-dielectric zero-index optical metamaterial. *Nature Photonics* **2013**, *7* (10), 791-795. DOI: 10.1038/nphoton.2013.214.

(76) Lobet, M.; Liberal, I.; Knall, E. N.; Alam, M. Z.; Reshef, O.; Boyd, R. W.; Engheta, N.; Mazur, E. Fundamental Radiative Processes in Near-Zero-Index Media of Various Dimensionalities. *ACS*

Photonics **2020**, *7* (8), 1965-1970. DOI: 10.1021/acsphotonics.0c00782.

(77) Caligiuri, V.; Palei, M.; Imran, M.; Manna, L.; Krahne, R. Planar double-epsilon-near-zero cavities for spontaneous emission and Purcell effect enhancement. *ACS photonics* **2018**, *5* (6), 2287-2294.

(78) Akahane, Y.; Asano, T.; Song, B.-S.; Noda, S. High-Q photonic nanocavity in a two-dimensional photonic crystal. *Nature* **2003**, *425* (6961), 944-947.

(79) Chow, E.; Lin, S.; Johnson, S.; Villeneuve, P.; Joannopoulos, J.; Wendt, J. R.; Vawter, G. A.; Zubrzycki, W.; Hou, H.; Alleman, A. Three-dimensional control of light in a two-dimensional photonic crystal slab. *Nature* **2000**, *407* (6807), 983-986.

(80) Ogawa, S.; Imada, M.; Yoshimoto, S.; Okano, M.; Noda, S. Control of light emission by 3D photonic crystals. *Science* **2004**, *305* (5681), 227-229.

(81) Tsai, A.-P.; Guo, J.; Abe, E.; Takakura, H.; Sato, T. J. A stable binary quasicrystal. *Nature* **2000**, *408* (6812), 537-538.

(82) Riklund, R.; Severin, M.; Liu, Y. The Thue-Morse aperiodic crystal, a link between the Fibonacci quasicrystal and the periodic crystal. *International Journal of Modern Physics B* **1987**, *1* (01), 121-132.

(83) Staliunas, K.; Sánchez-Morcillo, V. J. Spatial filtering of light by chirped photonic crystals. *Physical Review A* **2009**, *79* (5), 053807.

(84) Niu, S.; Huyan, H.; Liu, Y.; Yeung, M.; Ye, K.; Blankemeier, L.; Orvis, T.; Sarkar, D.; Singh, D. J.; Kapadia, R. Bandgap control via structural and chemical tuning of transition metal perovskite chalcogenides. *Advanced Materials* **2017**, *29* (9), 1604733.

(85) Majumdar, A.; Kim, J.; Vuckovic, J.; Wang, F. Electrical control of silicon photonic crystal cavity by graphene. *Nano Lett* **2013**, *13* (2), 515-518. DOI: 10.1021/nl3039212.

(86) Yi, S.; Zhou, M.; Yu, Z.; Fan, P.; Behdad, N.; Lin, D.; Wang, K. X.; Fan, S.; Brongersma, M. Subwavelength angle-sensing photodetectors inspired by directional hearing in small animals. *Nature Nanotechnology* **2018**, *13* (12), 1143-1147.

(87) Eguchi, K.; Enomoto, S.; Furuno, K.; Goldman, J.; Hanada, H.; Ikeda, H.; Ikeda, K.; Inoue, K.; Ishihara, K.; Itoh, W. First results from KamLAND: evidence for reactor antineutrino disappearance. *Physical Review Letters* **2003**, *90* (2), 021802.

(88) Mell, P.; Grance, T. The NIST definition of cloud computing. **2011**.

Enhancing large-area scintillator detection with photonic crystal cavities

Wenzheng Ye[1,2], Gregory Bizarri[3], and Muhammad D. Birowosuto[4]*, Liang Jie Wong[1,2]*

[1]School of Electrical and Electronic Engineering, Nanyang Technological University, 50 Nanyang Avenue, Singapore 639798, Singapore

[2]CNRS-International-NTU-THALES Research Alliance (CINTRA), Nanyang Technological University, 50 Nanyang Drive, 637553, Singapore

[3]Cranfield University, Bedfordshire, MK43 0AL, England

[4]Łukasiewicz Research Network-PORT Polish Center for Technology Development, Stabłowicka 147, 54-066 Wrocław, Poland

*Email: muhammad.birowosuto@prasetiyamulya.ac.id

*Email: liangjie.wong@ntu.edu.sg

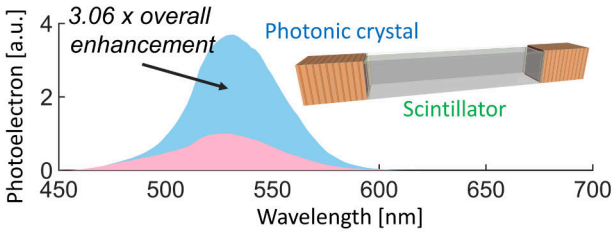

One-dimensional photonic crystal cavities – added externally to scintillator materials – can be used to enhance the overall photodetector signal by 3 times.

Enhancing large-area scintillator detection with photonic crystal cavities

Ye, Wenzheng

2022-12-21

Ye W, Bizarri G, Birowosuto MD, Wong LJ. (2022) Enhancing large-area scintillator detection with photonic crystal cavities. ACS Photonics, Volume 9, Issue 12, December 2022, pp. 3917-3925
https://doi.org/10.1021/acsphotonics.2c01235